# AUTOMATIC SEGMENTATION OF OPTIC DISC USING AFFINE SNAKES IN GRADIENT VECTOR FIELD

*Sidhartha Dey* ⋆, *Kapil Tahiliani* ⋆, *J. R. Harish Kumar* ⋆ †, *A. K. Pediredla* ⋄, *Chandra Sekhar Seelamantula* †

⋆ Department of Electrical and Electronics Engineering, Manipal Institute of Technology, Manipal, India
† Department of Electrical Engineering, Indian Institute of Science, Bangalore, India
⋄ Department of Electrical and Computer Engineering, Rice University, Houston, USA
E-mails:{sidhartha.dey1996, tahilianikapil1995}@gmail.com, {harishj, chandrasekhar}@iisc.ac.in,
aditya.eee.nitw@gmail.com

## ABSTRACT

The optic disc is one of the prominent features of a retinal fundus image, and its segmentation is a critical component in automated retinal screening systems for ophthalmic anomalies, such as diabetic retinopathy and glaucoma. In this paper, we propose a novel method for optic disc segmentation using affine snakes, where the snake evolves using an affine transformation and requires a priori knowledge of the desired object shape. We determine the affine transformation parameters by first computing a force field on the image and then deforming the snake till the net force on the snake is zero. The affine snakes technique excels in its speed of convergence. This is attributed to the fact that only six parameters require optimization, the six parameters being the horizontal and vertical scaling, shearing and translation components of an affine transformation. Localization of the optic disc is done using normalized cross-correlation and segmentation is done using the affine snakes technique. This technique is tested on publicly available fundus image datasets, such as IDRiD, Drishti-GS, RIM-ONE, DRIONS-DB, and Messidor, with Dice Indices of 0.943, 0.958, 0.933, 0.913, and 0.912, respectively.

***Index Terms*—** Affine snakes, optic disc, segmentation, affine transformation, gradient vector field

## 1. INTRODUCTION

The optic disc (OD), also known as the optic nerve head, is the area of the retina where the optic nerve leaves the eye. As it does not contain any sensory receptors, it is called the blind spot in the eye. Physical appearance of the OD include its shape, which is approximately circular, and its color, which ranges from orange to bright yellow to even whitish. Optic disc detection/localization and segmentation is a crucial component in retinal analysis [1], [2]. It can help in locating the fovea which is determined to be a fixed distance from the OD centre, segmenting blood vessels using the OD as a seed point, removing or suppressing the OD in order to better locate retinal exudates, and monitoring changes in the appearance and morphology of the OD, including the cup-to-disc ratio examination, in order to effectively diagnose glaucoma.

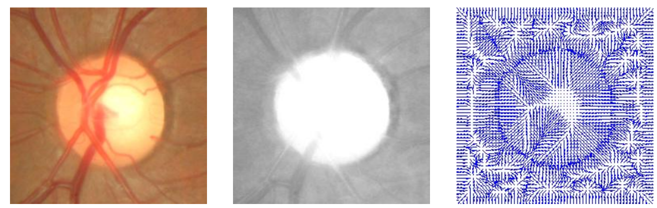

(a) (b) (c)

**Fig. 1**. [Color online] Optic disc in a (a) cropped fundus image; (b) red channel image; (c) GVF image

### 1.1. Related Work

Over the years, numerous state-of-the-art techniques have been proposed, all varying in theoretical modelling and approach. Discussing some of the state-of-the-art techniques which have emerged in the last few decades, we start with Morales et al., who made use of principal component analysis (PCA) and morphological operations as preprocessing steps to detect the centroid of the OD followed by watershed transformations and circle fitting technique to segment the OD boundary [3]. Aquino et al. approximated the OD boundary using mathematical morphology, edge detection techniques and circular Hough transform (CHT) [2]. In a recent paper, Zahoor et al. made use of morphological operations and CHT as preprocessing and OD localization techniques, respectively, and implemented polar transform-based adaptive thresholding to segment the OD [4]. Cheng et al. proposed a superpixel approach in which histogram analysis and centre surround statistics were used to classify the OD [5]. Walter et al. automated OD detection using morphological filtering techniques and segmentation using the watershed transformation [6]. Dashtbozorg et al. introduced a sliding-band filter (SBF) for the segmentation of OD [7]. Sigut et al. used retinal vessels information and boundary approximation to localize and segment the OD, respectively [8]. Lowell et al. used a modified version of Hu's circular deformable active contour model [9], incorporating an elliptical global model, to segment the OD [10]. Joshi et al. modified the region-based active contour model and traditional Chan-Vese model [11] by incorporating local image information around points of interest [12]. Kumar et al. defined a local contrast function based active disc model which was then minimized to find the OD boundary [13]. Recently, methods have made use of machine learning methods, such as those proposed by Sevastopolsky [14] and Zilly et al. [15]. Sevastopolsky used a convolution neural network (CNN) based on U-Net [16], which take an input image and produces an output probability map, as the core of the method with contrast limited adaptive histogram equalization (CLAHE) as a preprocessing step [14]. Zilly et al. proposed an ensemble learning method inspired by CNNs and made use of boosting and entropy sampling to improve the training of the network [15].

### 1.2. Our Contribution

In this paper, we propose an automated method of OD segmentation using affine snakes in a gradient vector field (GVF). For the formulation of affine snakes in a GVF, we drew inspiration from the unified approach of snakuscules and ovuscules by Pediredla et al. [17]. In their work, they too evolved the snakuscule/ovuscule through an affine transformation. However, they derive the partial derivatives with respect to a normalized contrast function. This is followed by the initialization of the active contour which then undergoes an affine transformation to give the final segmentation result. Normalized cross-correlation technique is used for the automatic localization of the OD [18]. The proposed snake features only six degrees-of-freedom, thereby enabling it to be computed faster than state-of-the-art methods.

## 2. PROPOSED METHODOLOGY

The method proposed proceeds as follows: detect/localize the OD and determine the centre coordinates, crop out the OD from the fundus image using the centre coordinates and a priori knowledge of the size (an approximation), calculate the GVF from the red channel of the OD and finally compute the affine transform using the optimized parameters calculated in Subsection 2.3. The affine snakes algorithm functions on the assumption that the initial contour can be mapped to the final contour by an affine transformation. As an affine transform contains six, free parameters, we need to solve for six variables, which we do using gradient descent technique. By calculating the partial derivatives and updating the affine parameters, the snake evolves to obtain the final segmentation. However, initialization of the contour is still imperative and so, before using affine snakes for OD segmentation, we first localize the OD using normalized cross-correlation technique [18] and then proceed with affine snakes in GVF.

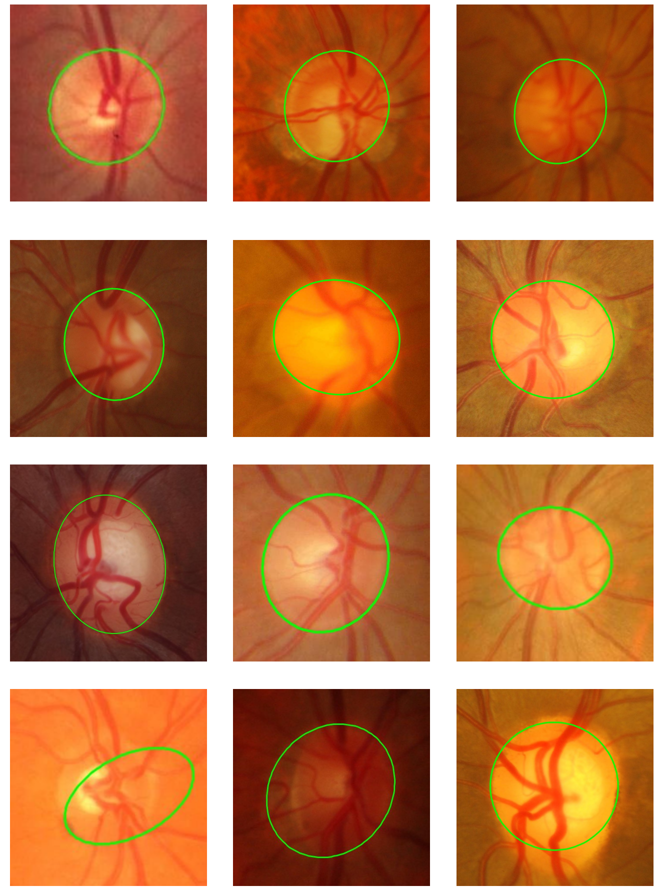

**Fig. 2**. [Color online] Figures in first three rows showing good segmentation results. Figures in fourth row show failed segmentation.

### 2.1. The Gradient Vector Field (GVF)

The GVF forms part of the foundation of the algorithm. Proposed by Xu and Prince [19], the GVF offers a larger capture range and can force the snake into concavities better than a conventional vector field. Effectively, the GVF acts as a force which moves the snake in 6-D space (six parameters) as the horizontal and vertical vector field components are what influence the values of the partial derivatives calculated in Subsection 2.3. It is important that the vector field is present wherever in the image the snake may be initialized to prevent stagnation of the snake. This requirement makes the GVF the ideal choice for the algorithm and so is calculated, using equations (1) for the red channel of the cropped OD after preprocessing, as shown in Fig. 1. The red channel is chosen as the OD boundary is the most prominent in this channel, which then gives rise to an accurate GVF. The GVF defined by [19] is a vector field $\mathbf{v}(x, y) = [u(x, y)\, v(x, y)]$ that minimizes the following cost:

$$\varepsilon = \iint |\nabla f|^2 \underbrace{|\mathbf{v} - \nabla f|^2}_{\text{SE}} + \mu \underbrace{({u_x}^2 + {u_y}^2 + {v_x}^2 + {v_y}^2)}_{\text{Regularization}}\, \mathrm{d}x\, \mathrm{d}y, \tag{1}$$

where SE represents the squared error loss functional that penalizes the vector field for deviating from the gradient image $\nabla f(x, y)$. $u_x$, $u_y$, $v_x$, $v_y$ represent the partial derivatives of horizontal and vertical components of the vector field in $x$ and $y$ directions. The regularization term forces the vector field to be smooth. The squared error loss functional and regularization term are combined after weighting with $|\nabla f|^2$ and $\mu$, respectively. This combination will ensure that the vector field is close to gradient image when the gradient values are strong and the vector field is continuous in the remaining cases. The regularization parameter $\mu$ governs the effect of smoothing and should be set according to the amount of noise present in the image (more noise requires larger $\mu$ value). Minimization of the energy function defined in (1) results in a GVF that is directed to the nearest edge.

### 2.2. Affine Snakes

The initial contour is defined as $\mathbf{r}(t) = (x(t), y(t))$, where $t \in C$ represents the collection of points. For $C = \mathbb{R}$, $(x(t), y(t))$ represents a continuous set of points, and for $C = \mathbb{Z}$, the shape consists of a discrete set of points. We assume that $\mathbf{r}(t)$ is in the counter-clockwise direction. The shape of the contour after an affine transformation is given by:

$$\mathbf{R}(t) = \begin{pmatrix} X(t) \\ Y(t) \end{pmatrix} = \begin{pmatrix} A & B \\ C & D \end{pmatrix} \begin{pmatrix} x(t) \\ y(t) \end{pmatrix} + \begin{pmatrix} x_c \\ y_c \end{pmatrix} \tag{2}$$

The optimal values of parameters $A, B, C, D, x_c$, and $y_c$ achieve the final segmentation.

### 2.3. Parameter Optimization

The partial derivatives $\mathrm{d}A, \mathrm{d}B, \mathrm{d}C, \mathrm{d}D, \mathrm{d}x_c$, and $\mathrm{d}y_c$ usher the snake towards the object boundaries. The role played by each of the parameters is examined and the corresponding differentials are formulated as a result. We perform an inverse affine transformation to vector field $\mathbf{v}$ such that the template remains in its initial configuration. The transformed vector field is represented as $\mathbf{V}$. This results in the following equality:

$$\mathbf{V}(\mathbf{r}(t)) = \mathbf{v}(\mathbf{R}(t)) \tag{3}$$

**Table 1**. Segmentation performance of the proposed method

| Dataset | $J_I$ [1] | $D_I$ [2] | $S_E$ [3] | $S_P$ [4] | $A_T$ [5] (s) |
|---|---|---|---|---|---|
| IDRiD | 0.896 | 0.943 | 0.923 | 0.999 | 3.635 |
| Drishti-GS | 0.921 | 0.958 | 0.932 | 0.999 | 2.026 |
| RIM-ONE | 0.880 | 0.933 | 0.953 | 0.961 | 1.472 |
| Messidor | 0.857 | 0.912 | 0.924 | 0.976 | 1.020 |
| DRIONS-DB | 0.850 | 0.913 | 0.919 | 0.997 | 0.410 |

[1] Jaccard Index [2] Dice Index [3] Sensitivity [4] Specificity
[5] Average run-time

Parameter $A$ scales the snake in x-direction. Hence, the horizontal component of the vector field will affect this parameter.

$$\begin{aligned} \mathrm{d}A &= \oint_{\mathbf{r}} \mathrm{d}\mathbf{r}(t) \times (\mathbf{V}_x(\mathbf{r}(t)),\, 0).\mathbf{k} \\ \Rightarrow \mathrm{d}A &= \oint_{\mathbf{R}} \mathrm{d}\mathbf{r}(t) \times (\mathbf{v}_x(\mathbf{R}(t)),\, 0).\mathbf{k} \\ &= \oint_{\mathbf{R}} \mathbf{v}_x(\mathbf{R}(t))\mathrm{d}y \end{aligned} \tag{4}$$

where $\mathbf{k}$ is the unit vector along the z-axis. Parameter $B$ shears the snake in the horizontal direction. Hence, its partial derivative is calculated as follows:

$$\begin{aligned} \mathrm{d}B &= -\oint_{\mathbf{R}} \mathrm{d}\mathbf{r}(t) \cdot (\mathbf{v}_x(\mathbf{R}(t)),\, 0) \\ &= -\oint_{\mathbf{R}} \mathbf{v}_x(\mathbf{R}(t))\mathrm{d}x \end{aligned} \tag{5}$$

Similarly, $C$ and $D$ are given by:

$$\begin{aligned} \mathrm{d}C &= \oint_{\mathbf{R}} \mathrm{d}\mathbf{r}(t) \cdot (0,\, \mathbf{v}_y(\mathbf{R}(t))) \\ &= \oint_{\mathbf{R}} \mathbf{v}_y(\mathbf{R}(t))\mathrm{d}y \end{aligned} \tag{6}$$

$$\begin{aligned} \mathrm{d}D &= -\oint_{\mathbf{R}} \mathrm{d}\mathbf{r}(t) \times (0,\, \mathbf{v}_y(\mathbf{R}(t))).\mathbf{k} \\ &= -\oint_{\mathbf{R}} \mathbf{v}_y(\mathbf{R}(t))\mathrm{d}x \end{aligned} \tag{7}$$

Here, $C$ shears the snake in the vertical direction and, analogous to $A$, $D$ scales the snake in the vertical direction. Hence, they are both affected by the vertical component of the vector field. The differentials, with respect to the centre of the affine snake $(x_c, y_c)$, are independent of the snake orientation and are instead dependent only on the net magnitude evolving the snake. Hence,

$$\mathrm{d}x_c = \oint_{\mathbf{R}} \mathbf{v}_x(\mathbf{R}(t))\mathrm{d}\|\mathbf{r}(t)\| \tag{8}$$

$$\mathrm{d}y_c = \oint_{\mathbf{R}} \mathbf{v}_y(\mathbf{R}(t))\mathrm{d}\|\mathbf{r}(t)\| \tag{9}$$

**Table 2**. Performance comparison ($D_I$) with state-of-the-art techniques.

| Method | IDRiD (54) | RIM-ONE (169) | Drions-DB (110) | Drishti-GS (50) | Messidor (1200) |
|---|---|---|---|---|---|
| Zahoor et al. [4] | – | 0.8491 | 0.9378 | – | 0.9039 |
| Cheng et al. [5] | – | – | – | – | 0.933 |
| Aquino et al. [2] | – | – | – | – | 0.92 |
| Joshi et al. [12][20] | – | – | – | 0.96 | – |
| Kumar et al. [13] | – | – | 0.8380 | 0.9077 | 0.8456 |
| Walter et al. [6] | – | – | 0.6813 | – | – |
| Morales et al. [3] | – | – | 0.9084 | – | 0.8950 |
| Dashtbozorg et al. [7] | – | – | – | – | 0.9373 |
| Zilly et al. [15] | – | 0.942 | – | 0.973 | 0.947 |
| Sigut et al. [8] | – | – | – | – | 0.954 |
| Sevastopolsky [14] | – | 0.95 | 0.94 | – | – |
| **Proposed method** | **0.94357** | **0.93308** | **0.91316** | **0.95868** | **0.91257** |

Once the partial derivatives are calculated, the affine parameters are updated by the following equation:

$$Q_{n+1} = Q_n + \gamma \mathrm{d}Q \tag{10}$$

where $Q$ is a placeholder for $A, B, C, D, x_c$ or $y_c$ and $\gamma$ is the learning rate. After the affine parameters are updated, the contour is evolved using (2). The partial derivatives are recalculated and the process continues until the effect of the force field is minimized. The result is the optimal parameters for the affine snake.

## 3. EXPERIMENTAL RESULTS

An ImageJ [21] plugin was created and run as a batch process on publicly available fundus image datasets [22], [20], [23], [24], [25], and [26]. The segmentation results of the cropped, fundus images from the datasets are shown in Fig. 2. The failures in the last row of Fig. 2 are attributed to the lack of variation in colour causing low visibility of the OD, which becomes even more apparent in the red channel. The last image is the result of stronger boundaries lying away from the OD boundary. The Jaccard index ($J_I$), Dice index ($D_I$), sensitivity ($S_E$), specificity ($S_P$), and average run-time ($A_T$) were used to measure the performance of the proposed technique. As [25] and [24] had multiple experts prepare the ground truth reference images, we show the mean of the similarity scores. The $A_T$ of the algorithm is directly proportional to the resolution of the images, with more time required to compute the GVF of higher resolution images. The performance of the proposed algorithm is compared with the existing state-of-the-art techniques as shown in Table 2. The results of the state-of-the-art techniques were taken from publications cited in the "Method" column. From these results, we see that the affine snakes performs quite competitively with and surpasses most methods listed. Also when comparing the performance over multiple datasets, we see more consistency with affine snakes compared to other methods. For example, although [4] performs better than affine snakes on the Drions-DB dataset, the difference in performance when comparing other datasets, like RIM-ONE, sees affine snakes performing better and more consistently across different datasets. Hence, affine snakes is more reliable to use on different datasets. While affine snakes falls short compared to learning techniques like [14] and [15], the hardware utilized in them, an NVIDIA GRID Kepler GK104 GPU and Intel Xeon E5-2670 CPU [14] and a 2.66 GHz quad core CPU [15], is more sophisticated and not as easily accessible compared to the Intel i5, 4$^{\text{th}}$ generation CPU used to implement the proposed algorithm. While [14] proclaims a prediction time of 0.1s on average, the prediction time for [15] is 5.3s on average, which is significantly greater than the affine snakes average run-time for any dataset. Also, taking into account training and testing time for learning methods, affine snakes is faster to calibrate and execute with minimal "training" time as it processes each image with only basic a priori shape knowledge.

## 4. CONCLUSIONS

Optic disc segmentation is an important part of analyzing retinal images and automating this process allows mass processing of countless fundus images effortlessly. In this paper, we present a novel technique for optic disc segmentation using affine snakes in GVF. While this technique shows great promise, with similarity indices of 0.9+, we feel it can be refined even further to become one of the best non-learning segmentation techniques which requires minimal hardware and can even run on smart phones, an intended target platform. Future work will be to improve the accuracy of the proposed method. From our technique, the time-consuming or rate-limiting step is the GVF calculation and so ways to reduce this computation time will also be looked into. Further efforts include formalizing the affine snakes framework and testing it in hospitals to assist medical professionals.

## 5. REFERENCES


[1] S. Lu, "Accurate and efficient optic disc detection and segmentation by a circular transformation," *IEEE Trans. on Med. Imaging*, vol. 30, no. 12, pp. 2126–2133, 2011.

[2] A. Aquino, M. E. Gegndez-Arias, and D. Marn, "Detecting the optic disc boundary in digital fundus images using morphological, edge detection, and feature extraction techniques," *IEEE Trans. on Med. Imaging*, vol. 29, no. 11, pp. 1860–1869, 2010.

[3] S. Morales, V. Naranjo, J. Angulo, and M. Alcaiz, "Automatic detection of optic disc based on pca and mathematical morphology," *IEEE Trans. on Med. Imaging*, vol. 32, no. 4, pp. 786–796, 2013.

[4] M. N. Zahoor and M. M. Fraz, "Fast optic disc segmentation in retina using polar transform," *IEEE Access*, vol. 5, pp. 12293–12300, 2017.

[5] J. Cheng et al., "Superpixel classification based optic disc and optic cup segmentation for glaucoma screening," *IEEE Trans. on Med. Imaging*, vol. 32, no. 6, pp. 1019–1032, 2013.

[6] T. Walter, J. C. Klein, P. Massin, and A. Erginay, "A contribution of image processing to the diagnosis of diabetic retinopathy-detection of exudates in color fundus images of the human retina," *IEEE Transactions on Medical Imaging*, vol. 21, no. 10, pp. 1236–1243, 2002.

[7] B. Dashtbozorg, A. M. Mendonça, and A. Campliho, "Optic disc segmentation using the sliding band filter," *Computers in Biology and Medicine*, vol. 56, pp. 1–12, 2015.

[8] Sigut et al., "Contrast based circular approximation for accurate and robust optic disc segmentation in retinal images," *PeerJ*, vol. 5:e3763, 2017.

[9] Hu et al., "Vessel boundary extraction based on a global and local deformable physical model with variable stiffness," *Magn. Reson. Imag.*, vol. 16, no. 8, pp. 943–951, 1998.

[10] Lowell et al., "Optic nerve head segmentation," *IEEE Trans. on Med. Imaging*, vol. 23, no. 2, pp. 256–264, 2004.

[11] T. F. Chan and L. A. Vese, "Active contours without edges," *IEEE Trans. on Image Proc.*, vol. 10, no. 2, pp. 266–277, 2001.

[12] G. D. Joshi, J. Sivaswamy, and S. R. Krishnadas, "Optic disk and cup segmentation from monocular color retinal images for glaucoma assessment," *IEEE Trans. on Med. Imaging*, vol. 30, no. 6, pp. 1192–1205, 2011.

[13] J. R. H. Kumar, A. K. Pediredla, and C. S. Seelamantula, "Active discs for automated optic disc segmentation," *in Proc. IEEE GlobalSIP*, pp. 225–229, 2015.

[14] A. Sevastopolsky, "Optic disc and cup segmentation methods for glaucoma detection with modication of u-net convolutional neural network," *Pattern Recognition and Image Analysis*, vol. 27, no. 3, pp. 618–624, 2017.

[15] J. Zilly, J. M. Buhmann, and D. Mahapatra, "Glaucoma detection using entropy sampling and ensemble learning for automatic optic cup and disc segmentation," *Computerized Medical Imaging and Graphics*, vol. 55, pp. 28–41, 2017.

[16] O. Ronneberger, P. Fischer, and T. Brox, "U-net: Convolutional networks for biomedical image segmentation," *in International Conference on MICCAI*, vol. 9351, pp. 234–241, 2015.

[17] A. K. Pediredla and C. S. Seelamantula, "A unified approach for optimization of snakuscules and ovuscules," *in Proc. IEEE ICASSP*, pp. 681–684, 2012.

[18] J. R. H. Kumar et al., "A unified approach for detection of diagnostically significant regions-of-interest in retinal fundus images," *in Proc. IEEE TENCON*, pp. 19–24, 2017.

[19] C. Xu and J. Prince, "Snakes, shapes, and gradient vector flow," *IEEE Trans. on Image Proc.*, vol. 7, pp. 359–369, 1998.

[20] J. Sivaswamy et al., "A comprehensive retinal image dataset for the assessment of glaucoma from the optic nerve head analysis.," *JSM Biomedical Imaging Data Papers*, vol. 2, no. 1, pp. 1–7, 2015.

[21] NIH, "ImageJ," *https://imagej.nih.gov/ij/*.

[22] Porwal et al., "Indian diabetic retinopathy image dataset (IDRiD): A database for diabetic retinopathy screening research," *Data*, vol. 3, no. 3, 2018.

[23] J. Sivaswamy et al., "Drishti-GS: Retinal image dataset for optic nerve head (ONH) segmentation," *in Proc. IEEE ISBI*, pp. 53–56, 2014.

[24] E. J. Carmona, M. Rincón, J. García-Feijoó, and J. M. Martínez de-la Casa, "Identification of the optic nerve head with genetic algorithms," *Artificial Intelligence in Medicine*, vol. 43, no. 3, pp. 243–259, 2008.

[25] F. Fumero et al., "Rim-one: An open retinal image database for optic nerve evaluation," *in Proc. International Symposium on CBMS*, pp. 1–6, 2011.

[26] Decencire et al., "Feedback on a publicly distributed database: the messidor database," *Image Analysis & Stereology*, vol. 33, no. 3, pp. 231–234, 2014.